

Accounts

Molecular Basis for Transition-State Stabilization in Catalytic Antibodies

Takeshi Tsumuraya and Ikuo Fujii*

Department of Biological Science, Graduate School of Science, Osaka Prefecture University, 1-2 Gakuen-cho, Naka-ku, Sakai, Osaka 599-8570

Received May 8, 2008; E-mail: fujii@b.s.osakafu-u.ac.jp

Antibodies elicited against rationally designed transition-state analogs catalyze a large number of reactions, including many that cannot be achieved by standard chemical methods. This account describes a detailed investigation of the molecular mechanism of catalysis in catalytic antibodies. We have investigated the biochemical properties within a panel of six hydrolytic catalytic antibodies elicited against a phosphonate transition-state analog. The transition-state analyses (k_{cat}/k_{uncat} versus K_m/K_i) displayed a linear relationship with five antibodies, 6D9, 8D11, 4D5, 3G6, and 9C10, which have homologous primary amino acid sequences, while antibody 7C8 deviates from the linear relationship. These results suggest that the five antibodies catalyze the hydrolysis by the same reaction mechanism of transition-state stabilization and that catalytic factors other than transition-state stabilization are involved for antibody 7C8. The structure of 6D9 Fab with the transition-state analog (TSA) has been solved, showing that 6D9 binds the phosphonate of TSA by forming one hydrogen bond with His^{L27d}. The kinetic, structural, and thermodynamic analyses of 6D9 indicate that this antibody provides an efficient catalyst by transition-state stabilization through the hydrogen bond with His^{L27d} and the destabilization of the substrate. Although catalytic antibodies are still much inferior to natural enzymes in their catalytic efficiency, several aspects including the mechanism of enzyme catalysts can be faithfully mimicked. Therefore, the molecular mechanism of catalytic antibodies might provide useful insights to understanding the catalysis in enzymes.

1. Introduction

Both antibodies and enzymes play an important role in biological systems. These proteins are able to bind a large number of compounds, ranging from small molecules to macromolecules, with high affinity and specificity. Although enzymes can accelerate biological reactions, antibodies generally cannot. Pauling was the first to note that the difference between the two is that enzymes have evolved to selectively bind the transition state in the chemical transformations and are selected based on catalytic efficiency, whereas antibodies have evolved to maximize affinity for molecules in the ground state.[1–3] In 1969, Jencks predicted that stable molecules resembling the transition state of a reaction might be used as haptens to generate antibodies with tailored catalytic activities and selectivities.[4] Implementation of this idea was made possible by the development of monoclonal antibody techniques and in 1986 Lerner et al. and Schultz et al. independently reported antibody catalysis for the hydrolysis of aryl esters and carbonates, respectively.[5,6] These antibodies were generated by immunization with putative transition-state analog (TSA), with the expectation that the induced antigen-combining site could be both geometrically and electronically complementary to the transition state. Since the mammalian immune system is characterized by an almost limitless potential for providing receptor-like molecules for virtually any chemical structure, catalytic antibodies can provide "tailor-made" catalysts for any chemical transformation, including reactions for which no natural counterparts exists.[7,8]

This account describes a detailed investigation of the molecular mechanism of antibody-catalyzed hydrolysis. The catalytic antibodies described here were elicited against a single phosphonate transition-state analog. Most of them use transition-state stabilization as a major catalytic mechanism as expected from the hapten design. We were interested in the molecular mechanism of transition-state stabilization that is one outstanding characteristic of enzymes and then have studied the detailed kinetic and thermodynamic binding properties and the crystal structures of the catalytic antibodies. These analyses allow us to visualize the mechanisms of transition-state stabilization as well as substrate destabilization. Although the catalytic antibodies are still much inferior to natural enzymes in their catalytic efficiency, several aspects of enzyme catalysis can be faithfully mimicked. Therefore, the molecular mechanism of the catalytic antibodies might provide useful insights to understand the catalysis in enzymes.

2. Parallels between Molecular Evolution of Enzymes and Antibodies

There are many parallels between the immunological evolu-

Published on the web September 11, 2008; doi:10.1246/bcsj.81.1039

Table 1. Similarities and Dissimilarities Found in Molecular Evolution of Enzymes and Antibodies

Molecular evolution of enzymes	Molecular evolution of antibodies
• Gene duplication and exon shuffling	• Random recombination of antibody genes (V, D, and J)
• Point mutation	• Somatic mutation
• Natural selection: catalytic activity	• Clonal selection: affinity
• Period: millions of years	• Period: several weeks

tion of antibodies and the evolutional process of enzymes (Table 1). Both processes involve genetic recombination and accumulated point mutations coupled with a selection process during which molecules with the desired functions are selected from a large library of proteins. In the case of enzymes, gene duplication and exon shuffling provide enzymes with new structures and functions.[9,10] Point mutations further increase molecular diversity and refine biological functions. Similar mechanisms are responsible for the diversity in the immune system.[11,12] Antibody genes are segmented and exist as groups with multiple members. For example, in the murine genome there are at least a hundred variable (V_H) segments, 15 diversity (D) segments, and five joining segments (J_H) for the heavy chain variable region, and hundreds of variable (V_k) segments and five joining segments (J_k) for the light chain variable region. Genes for the antibody heavy chains are assembled by the random recombination of V_H, D, J_H segments and those for the light chains are assembled by the random recombination of V_k and J_k segments. Moreover, the exact site of the joining between segments during gene recombination is imprecise and leads to junctional diversity. Nucleosides can be deleted from or added randomly to both ends of the D gene segments, leading to CDR H3 length variations and even greater variability at the joining region. After gene recombination, the germline antibody undergoes affinity maturation during which somatic mutations are introduced throughout the antibody variable region, further expanding the sequence diversity of the germline antibody repertoire. As a result, the immune system has the potential to generate more than 10^{12} unique antibodies.[13]

3. Transition-State Stabilization in Catalytic Antibodies

3.1 Transition-State Stabilization in Enzymes. A catalyst achieves rate acceleration by stabilizing the reaction's transition state instead of stabilizing the ground state. Chemical catalysts such as general acid–base, metal ions, charged and nucleophilic molecules stabilize the transition states to give large rate acceleration. A combination of these chemical catalysts and entropic factors can account for a large proportion of the magnitude of catalysis by enzymes. In addition to these catalytic factors, the most outstanding characteristic of enzymes is translating binding energy into catalysis even if the binding takes place remote from the reaction site.[4,14]

Transition-state theory[15] ascribes enzyme catalysis to the complementarity of the enzyme to the transition state, and not the substrate, of the catalyzed reaction. Figure 1 shows the energy profile of a reaction in the absence and the presence of an enzyme. Chemical transformation proceeds through the high-energy transition state ($S^{\neq}$) to give the products (P). In enzymatic reactions, an enzyme (E) strongly binds to the transition state to lower the activation energy (ΔG_{TS}) and catalyze

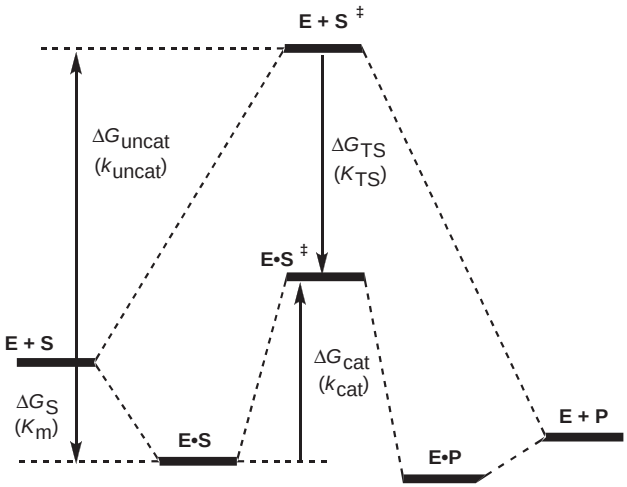

Figure 1. Energy profiles for the enzyme-catalyzed and uncatalyzed reactions.

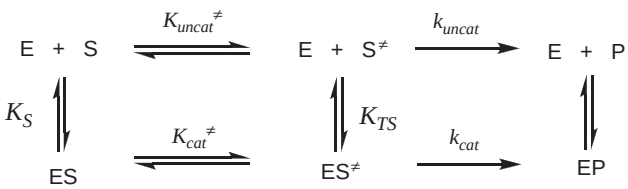

Figure 2. A thermodynamic cycle interrelating substrate (S) and transition-state ($S^{\neq}$) binding for an enzyme (E).

the reaction. On the other hand, an enzyme binds to the ground state of the substrate (S) very weakly. In other words, an enzyme achieves efficient catalysis by maximizing the differential binding affinities between the transition state (K_{TS}) and the substrate (K_S).

The relationship between transition-state stabilization and enzymatic catalysis is effectively illustrated by the thermodynamic cycle (Figure 2).[16–18] This thermodynamic box relates the dissociation constants of an enzyme with the substrate (K_S) and the transition state (K_{TS}) and the equilibrium constants $K_{uncat}^{\neq}$ and $K_{cat}^{\neq}$ for the uncatalyzed and the enzyme-catalyzed reactions, respectively (eq 1).

$$K_S/K_{TS} = K_{cat}^{\neq}/K_{uncat}^{\neq} \quad (1)$$

The rate of product formation (P) in the enzyme-catalyzed reaction can be considered proportional to the concentration of the transition state for this reaction, $ES^{\neq}$, and therefore the equilibrium constant for the formation of this species, $K_{cat}^{\neq}$, is as follows:

$$d[P]/dt = (kT/h)[ES^{\neq}] \quad (2)$$

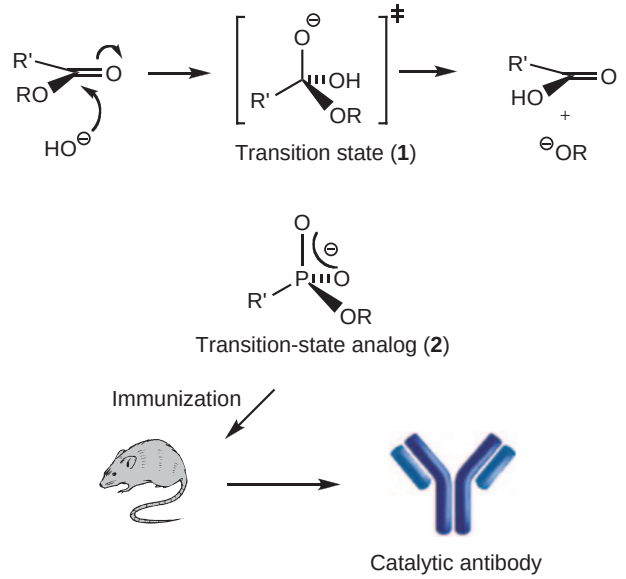

Figure 3. Generation of esterolytic catalytic antibodies by immunization of a phosphonate transition-state analog **2**.

and since $[ES^{\neq}] = K_{cat}^{\neq} \times [ES]$,

$$d[P]/dt = (kTK_{cat}^{\neq}/h)[ES] = k_{cat}[ES] \quad (3)$$

where k is the Boltzmann constant, T is temperature in Kelvin, and h is Planck's constant. The uncatalyzed rate is similarly proportional to $K_{uncat}^{\neq}$. Since the kinetic constants are proportional to their corresponding equilibrium constants, the ratio of k_{cat}/k_{uncat} can be inserted into eq 1 to afford eq 4.

$$K_S/K_{TS} = k_{cat}/k_{uncat} \quad (4)$$

The implication of eq 4 is significant: one can predict the rate enhancement of an enzyme-catalyzed reaction from the ratio of the affinity for the substrate relative to the affinity for the transition state.

3.2 Generation of Catalytic Antibodies. To generate catalysts like enzymes, it is essential to construct two sites in one molecule, a "recognition site" binding the substrate and a "reaction site" carrying out chemical transformation. Catalytic antibodies use the diversity of antibodies in the immune system to obtain the "recognition site." The next issue is how to construct the "reaction site" in the antigen-combining site. A number of strategies have been developed for generating catalytic antibodies, including (i) the use of antibodies to stabilize negatively and positively charged transition states, (ii) the use of antibodies as entropic traps, and (iii) the generation of antibodies with catalytic groups such as general acid–base catalysis in their combining sites. Among these the most successful approach is the generation of an antigen-combining site that can stabilize the transition state by immunization of a stable transition-state analog.[7]

The earliest successes in generation of catalytic antibodies were the alkaline hydrolysis of esters and carbonates. Figure 3 shows the strategy for generation of esterolytic antibodies by immunization with a phosphonate transition-state analog. The hydrolysis of esters involves formation of a tetrahedral, negatively charged transition state **1** that subsequently decomposes to provide the corresponding acid and alcohol. This high-energy transition state **1** can be mimicked effectively with a phosphonate **2**. Phosphonate compounds resemble the transition states in a number of ways, including tetrahedral geometry, negative charge, and increased bond lengths. Ab initio calculations also supported the hypothesis that phosphonate is an effective analog for the tetrahedral transition state in terms of its structure and charge.[19] Once the hapten has been designed and prepared, it is conjugated with a carrier protein keyhole limpet hemocyanin (KLH) or bovine serum albumin (BSA) to provide an antigen with sufficient immunogenicity. Antibodies elicited against the transition-state analog bind the transition state more strongly than the ground state of the substrate, leading to efficient catalysts. These transition-state analogs have been used widely as haptens to generate hydrolytic antibodies.[17,20–22]

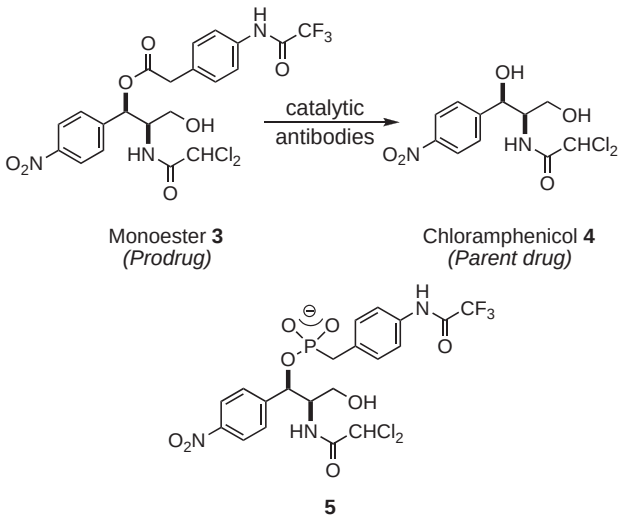

Figure 4. Prodrug activation via antibody-catalyzed reaction.

4. Generation of Catalytic Antibodies for Prodrug Activation

4.1 Generation of Catalytic Antibodies by Immunization of a Phosphonate Transition-State Analog. One goal of the study of catalytic antibodies is to generate tailor-made catalysts for applications in medicine. Although many reviews of catalytic antibody technology have described the possibilities of future applications, there have been no specific examples. An example of a possible use with catalytic antibodies is related to the action of prodrugs. If a catalytic antibody can activate a prodrug that is stable toward natural enzymes, it can be a site-specific drug delivery system. We succeeded in demonstrating the first example of prodrug activation via catalytic antibodies by using the antibiotic chloramphenicol as a model drug (Figure 4).[23] Furthermore, this idea has been expanded to examine antibody-directed abzyme prodrug therapy (ADAPT).[24]

Immunization with a keyhole limpet hemocyanin (KLH) conjugate of the phosphonate transition-state analog **5**, designed on the basis of the transition-state stabilization concept, provided 11 immunoglobulin G (IgG) proteins binding to the hapten **5**. Six of 11 antibodies were found to catalyze the hydrolysis of monoester **3** to provide chloramphenicol (**4**) with varying degrees of activity.

The most active antibody, 6D9, catalyzed the prodrug hydrolysis in a manner consistent with Michaelis–Menten kinetics with k_{cat} of 0.133 min^{-1} and K_m of 64 μM. Comparison of the k_{cat} value with the rate constant for the uncatalyzed reaction (k_{uncat}) gives ca. 900-fold acceleration. The antibody-catalyzed reaction using 2 μM antibody 6D9 was completely inhibited by the addition of 5 μM hapten **5**, demonstrating that catalysis takes place against monoester **3** in the antigen-combining site.

We then demonstrated the possibility of prodrug therapy by achieving inhibition of growth of *Bacillus subtilis* cells, which were inhibited by prodrug monoester **3** when combined with antibody 6D9. The antibody 6D9 catalyzed the reaction with multiple turnover to generate enough chloramphenicol to inhibit bacterial growth, as indicated by a clear inhibitory zone after incubation with the monoester (Figure 5). Using the same method, no inhibition was detected by incubation of either the monoester or the antibody alone. These results revealed that only the antibody hydrolytically activated the monoester, which can be expected to be a suitable prodrug, as it is resistant to the action of bacterial hydrolytic enzymes.

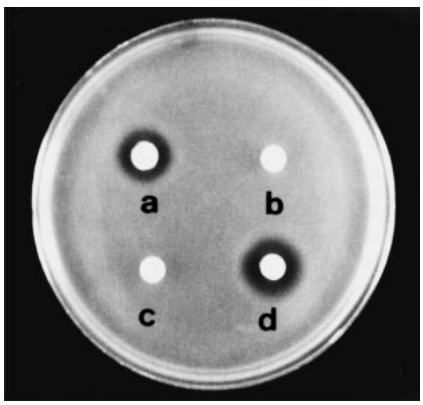

Figure 5. Growth inhibition assay of *Bacillus subtilis* ISW 1214 was performed by the paper-disc agar diffusion method: (a) 100 mM substrate plus 20 μM antibody, (b) 100 mM substrate alone, (c) 20 μM antibody alone, and (d) 2.0 mM chloramphenicol. An overnight culture (100 mL) of *Bacillus subtilis* ISW 1214 and melted top agarose (3.0 mL adjusted to pH 8.0 by addition of 1.0 M NaOH) were mixed and spread on a 90-mm LB agar plate. After each sample of 10 mL was applied to the 6.0-mm paper discs resting on the plates, the plates were placed at 37 °C for 18 h.

4.2 Molecular Recognition and Mechanism Displayed by Catalytic Antibodies. The diversity of the immune response can provide a panel of catalytic antibodies that possess varying degrees of catalytic activity and substrate specificity. These results have raised fundamental questions, such as the following: how do catalytic antibodies generated by immunization with a single hapten differ on a structural or mechanistic basis? Therefore, a central question in catalytic antibody research concerns the extent to which the rationally designed hapten dictates the paratopes for catalytic function in the antigen-combining site. We then studied the correlation between the antigen-combining structures and the chemical properties within a panel of catalytic antibodies elicited against a single hapten, which can potentially provide a more global understanding of the molecular mechanisms by which catalytic antibodies are generated in immune responses.[25]

4.2.1 Transition-State Analyses: To survey the catalytic activity within the six catalytic antibodies (6D9, 7C8, 8D11, 4B5, 9C10, and 3G6) elicited against the transition-state analog **5**, the kinetic parameters, including the K_i values against the transition-state analog **5**, of the antibody-catalyzed hydrolysis were determined (Figure 6 and Table 2). The K_i values against the transition-state analog correspond to the dissociation constants for the transition-state analog. In practice, the catalytic antibodies are identified among a panel of antibodies based on high binding constants for transition-state analogs. However, the results from comparison of the K_i values and the catalytic activities (k_{cat}) within the panel of antibodies indicate that antibodies with high binding affinity are not always highly catalytic. Figure 7 shows plots of $\log(k_{cat}/k_{uncat})$ versus $\log K_i$ for the six catalytic antibodies. There was no significant correlation between the catalytic activity and the affinity of the

Table 2. Kinetic Parameters of the *anti*-**5** Antibody-Catalyzed Hydrolysis of Substrate **6**[a)]

Antibody	k_{cat}/min^{-1}	$K_m/\mu M$	k_{cat}/k_{uncat}	K_i[b)]/nM	K_m/K_i
6D9	0.129	61.4	935	55.6	1104
7C8	0.115	3.8	833	298.0	13
8D11	0.034	2.6	244	15.7	165
4B5	0.032	3.7	230	17.0	217
9C10	0.008	0.9	56	14.0	42
3G6	0.006	1.3	47	38.3	33

a) Reaction conditions: 25 °C, 10% DMSO/50 mM TrisHCl, pH 8.0. The first-order rate constant of the hydrolysis reaction without antibody (k_{uncat}) was 1.38×10^{-4} min^{-1}. b) Against transion-state analog **5**.

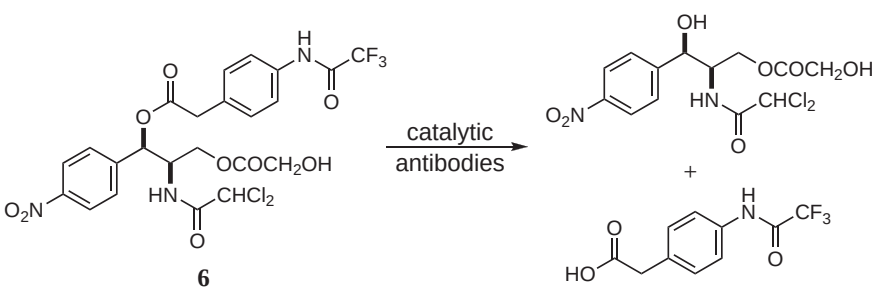

6

Figure 6. Antibody-catalyzed hydrolysis of ester substrate **6** used for kinetic measurements.

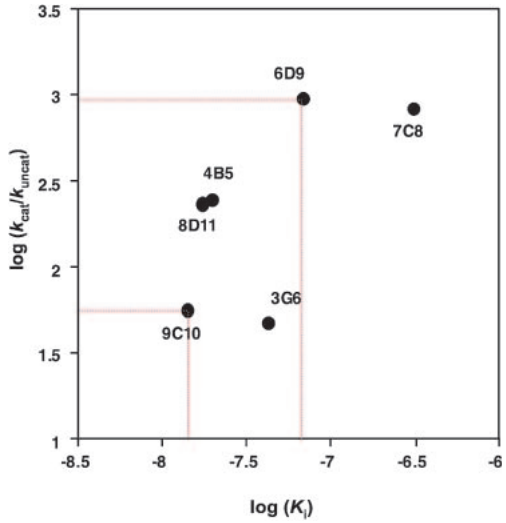

Figure 7. Plot of $\log(k_{cat}/k_{uncat})$ versus $\log K_i$ for the six catalytic antibodies elicited against transition-state analog **5**. There was no significant correlation between catalytic activities and the affinity of the transtion-state analog.

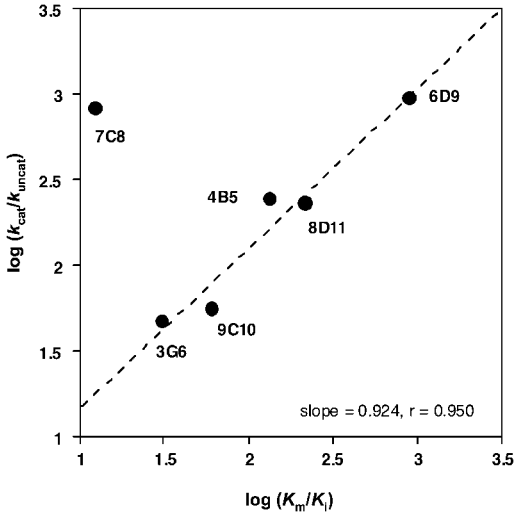

Figure 8. Plot of $\log(k_{cat}/k_{uncat})$ versus $\log(K_m/K_i)$ for catalytic antibodies generated against phosphonate transition-state analog **5**. A linear relationship was observed for antibodies 6D9, 8D11, 4B5, 9C10, and 3G6, suggesting that the antibody-combining sites act as catalysts by stabilizing the transition state.

transition-state analog. In the present study, increased catalytic activity of the six catalytic antibodies does not correlate with increased binding affinity to the transition-state analog. For example, the most active catalytic antibody, 6D9, has only moderate affinity for the transition-state analog, while the highest-affinity antibody, 9C10 has low catalytic activity among the six catalytic antibodies. Therefore, strong affinity to the transition state cannot maximize the reaction rates (k_{cat}).

According to transition-state theory, under ideal conditions, one can predict the rate enhancement of an antibody-catalyzed reaction from the ratio of the affinity for the substrate relative to the affinity for the transition state (eq 4). If a hapten is a true analog of the actual transition state of the reaction and contains no extraneous structural features that are not present in its corresponding substrate, K_S and K_{TS} can be estimated as Michaelis constant (K_m) and the inhibition constant for the transition-state analog (K_i), respectively. The ratio of K_m to K_i should then be equal to the rate enhancement ($k_{cat}/k_{uncat} = K_m/K_i$).[26]

Figure 8 shows plots of $\log(k_{cat}/k_{uncat})$ versus $\log(K_m/K_i)$ for the six catalytic antibodies.[24] Although the catalytic antibodies possess varying values of K_m, k_{cat}, and K_i, the transition-state analysis displays a linear relationship among antibodies 6D9, 8D11, 4G5, 9C10, and 3G6. The slope of the straight line is 0.924. This suggests that, in these five catalytic antibodies, the entire differential binding energy of the transition state to the ground state might be available for the rate enhancement. On the other hand, the plots for antibody 7C8 deviate from the linear relationship, suggesting that factors other than transition-state stabilization, such as a functioning acid, base or nucleophilic catalyst, are involved in the catalysis.

4.2.2 Amino Acid Sequence Analyses of Catalytic Antibodies: Immunization with a single haptenic transition-state analog generates a few catalytic antibodies among the dozens of antibodies capable of binding the hapten. The diversity of the immune response has raised some fundamental issues such as how do catalytic and noncatalytic antibodies differ on a structural basis? To address this issue, the variable region (V_L and V_H) primary sequences of 11 antibodies (including 6 catalytic and 5 noncatalytic antibodies) elicited against TSA **5** were deduced from the cDNA sequences (Figures 9 and 10).[27] The amino acid sequences of noncatalytic antibodies bear no relationship to one another, while the catalytic antibodies share significant structural identity. Furthermore, no catalytic antibodies possessing amino acid sequences with high homology to those of noncatalytic antibodies were detected. Five catalytic antibodies, 6D9, 8D11, 4B5, 9C10, and 3G6, showed 89–95% and 74–84% sequence identities in the complete light- and heavy-chain variable regions, respectively.

Antibody 7C8 was found to be exceptionally catalytic, but its structure was different from that of the other catalytic antibodies, with 55% and 44% amino acid sequence identities in the V_L and V_H regions, respectively, as compared to the prototype 6D9. This analysis suggests that 7C8 binds to the substrate or hapten in a mode of molecular interaction different from those of the other catalytic antibodies. In fact, examination of antibody-catalyzed reactions using various substrates demonstrated the substrate specificity of 7C8 to be different from that of the others as described in the next section.

4.2.3 Substrate Specificity: As shown in the previous section the catalytic antibodies 6D9, 8D11, 4B5, 9C10, and 3G6 (except 7C8) shared significant amino acid sequence identity to one another in the complete V_L and V_H regions, suggesting closely related structures in the antigen-combining site within these antibodies. Therefore, to confirm that the catalytic antibodies belong to a shared idiotype family in terms of combining-site structures and binding properties, the substrate specificity of the antibodies was examined using substrate **6** and its derivative **7**, in which the trifluoroacetyl group of **6** was converted to an acetyl group (Figure 11).[25a] If the combining-site structures and the binding modes to the hapten and the substrates of these catalytic antibodies are related to each

```
      1        10         20    27       30         40        50
                                 CDR1                          CDR2
6D9   ELVMTQTPLSLPVSLGDQASISCRSSQTIVHSNGDTYLDWFLQKPGQSPKLLIYKVSNRFS
4B5   ----------S----------------------N---E-Y--------------------
8D11  -------------------------------N--N---Q-Y--------N-----------
3G6   ---------------------Y-----S--Y-D-N---E-Y--------N-----------
9C10  --------------------------SL---S-N---E-Y--------------I-----

7C8   --------AT-S-TP--SV-L---A--SVSN.....K-H-YQ--SHE--R---KFA-QSIP

1G6   --------AT-S-TP--SV-L---A--S-SN-.....-H-YQ--SHE--R---KYT-QSI-
7A11  --------AI-S--P-ERV-F---A--SVGT.....NIH--Q--TNG--R---KYA-ESV-
6A6   --------A--S----QR-T----A-ESVDNYGISL.MN--Q-----P--V---AT--QG-
9B7   --------S-MS-----TV--T-HA-RV-SN.....NIG-LQ----K-I-G---HGT-LED
3A7   --------S-MYA---ERVT-T-KA--D-NS.....--S--H----K---S---RANTLLV


        60         70         80         90       100      109
                                          CDR3
6D9   GVPDRFSGSGSGTDFTLKISRVEAEDLGVYYCFQGSHVPPTFGGGTKLEIKRA
4B5   -------------------T---------------------------------
8D11  ------------------------------------------------------
3G6   -----------------N--T--------------L-F----------------
9C10  ----------------------------------T-------------------

7C8   -I-S--------S----S-NS--T--F-I-F-H-THGR-L---A-----L---

1G6   -I-F-------------T-NS--T--F-M-F-H-SNSW-L---A-----LN--
7A11  -I-S-------------S-NS--S--IAD---Q-SNNR-L---S-----L---
6A6   ---A-----------S-N-HP--ED-TAM-F-Q-SKEF-L---A-----L---
9B7   ---S--------A-YS-T--SL-S--FAD---V-YAQF-Y-------------
3A7   ---S--------Q-YS-T--SL-Y--M-L---L-YDEF-Y-------------
```

Figure 9. Deduced amino acid sequence comparison of V_L cDNA generated from *anti*-**5** monoclonal antibodies. Dashes denote identity to antibody 6D9 and dots, used to align sequences, represent no amino acid residues at a position. CDR designations and amino acids residue numbering are as described by Kabat et al.

```
      1        10        20        30        40          52       60
                                   CDR1                 CDR2
6D9   QVKLLESGGGLVKPGGSLKLSCAASGFTFSNYAMSWVRQTPEKRLEWVVSISSGG.SIYYL
4B5   ---------D--------------------S-G--------D-G----AT-TTD-TYT---
8D11  ---------D--------------------SFG--------DM-----AT--T-YIYT--S
3G6   ----------------------------T-V---------------AT-----RYT--P
9C10  -------------------------E----T-I--------------AT---S-TYT--R

7C8   --------AV-----A-V----KT------SSYIN-LK-K-GQS---IAW-YA-SGGTV-N

1G6   -----------------------------NT--V-------------A--------T--P
7A11  --------PE--R--ALV-I--K---Y--TDHYIN----K-GQG---IGW-YP-IND-K-N
6A6   --------PE-----A-V-M--RT--Y--TS-VIH--K-R-GQG-Q-IGY-NPYNDGTK-N
9B7   --------AE--RS-A-V----T----NIKD-YVH--K-G--QG-R-IGR-AP-NGDTV-A
3A7   --------AE-----A-V----TT---NIKDTYLH--K-R--QG---IGR-DPANGNTK-N


          70          82          90       100                 113
                                          CDR3
6D9   DSVKGRFTVSRDNARNILYLQMTSLRSEDTAMYFCARVSHYDGSRDWYFDVWGAGTSVTVSS
4B5   --------I-----K-T--------K-------Y---IPYVTYGGFYAM-Y--Q--------
8D11  --------I-----K-T-----S--K-----I---S-IPYLNSGGFYGM-H--Q--------
3G6   --------I---S-K-T-----S--------I-Y---RGNN....YD---Y--Q--TL----
9C10  --------------N-------S--------L-Y---RDY---.....-TY--Q--L----A

7C8   QHFTDKARLTV-TSSSTA-M-FS--TT--S-I-Y---YRYDE-.....-AY--Q--L----A

1G6   --------I---D---------S----------S-VS.........----------T-----
7A11  EKFR-KA-LTV-TSSSTA---LS--TF----V-----WTGGY-.....-AY--Q--L----A
6A6   EKF--KA-LTS-RSSRTA-MELS--T---S-V-Y---DKG..........Y--Q--TL----
9B7   PKFQ-KA-MTA-TSS-TA---LNI-T-----V-Y-NSKRG.........AY--Q--L----A
3A7   AKFL-KA--TI-TSS-TA--HLS--T-----V-Y-N...........--AN--Q--L----A
```

Figure 10. Comparison of the deduced amino acid sequences of V_H for 11 *anti*-**5** monoclonal antibodies. See legend to Figure 9 for symbol designation.

other, the antibodies should display a homologous substrate specificity.

Table 3 shows the relative velocities for substrate **6** and **7** in the antibody-catalyzed hydrolysis with the six catalytic antibodies. Antibodies 6D9, 8D11, 4B5, 9C10, and 3G6, with highly homologous amino acid sequences, displayed reduced catalytic activity for **7**, with rates 3.5–14 times lower than those for **6**. On the other hand, antibody 7C8, possessed substrate specificity different from those of the other catalytic antibodies to display the same activity against **6** and **7**. This

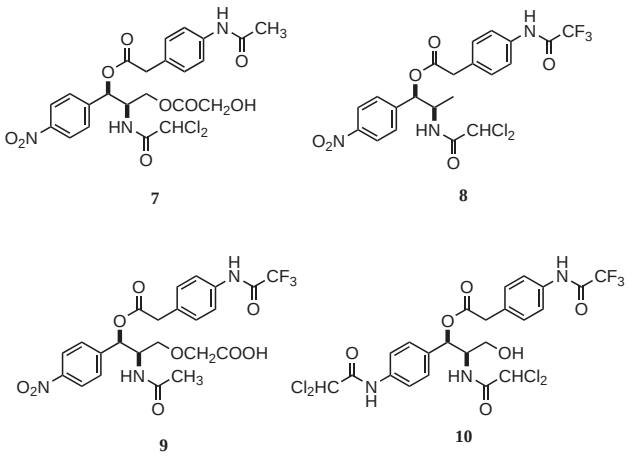

Figure 11. Structures of the substrates used in the substrate-specificity studies.

Table 3. Relative Efficiencies of *anti*-**5** Catalytic Antibodies for Hydrolysis of Substrate **6** and **7**[a)]

Antibody	Relative velocities[b)]	
	Substrate **6**	Substrate **7**
6D9	100	7
7C8	105	91
8D11	61	10
4B5	47	7
9C10	25	2
3G6	14	4

a) Reaction conditions: 5 μM of antibody and 200 μM of substrate in 10% DMSO/50 mM TirsHCl, pH 8.0, at 25 °C. b) Relative velocities were determined by comparing the hydrolysis of substrate **6** with antibody 6D9.

is consistent with the difference in the amino acid sequences of the *F*v regions.

In addition, we have examined the substrate specificity of prototype 6D9 in detail, using other substrates, **8**, **9**, and **10** (Figure 11). The kinetic parameters in the 6D9-catalyzed hydrolysis of substrates **7**, **8**, and **9** are shown in Table 4. Antibody 6D9 did not display catalytic activity for **10**, which bears a bulky *p*-dichloroacetamido group instead of the *p*-nitro group. Substrate **8** was found to be a good substrate for 6D9, with a K_m value and a rate enhancement (k_{cat}/k_{uncat}) comparable to those of **6**. Any structural change at the C-3 position should not affect the antibody–substrate interaction because the hapten was conjugated with the bulky carrier protein at the C-3 position. Catalytic antibody 6D9 had reduced hydrolytic activity with substrate **9**, which has an acetylamide derivative at the C-2 position. As noted above, 6D9 displayed reduced catalytic activity in the hydrolysis of substrate **7**. This suggests that the *p*-(*N*-trifluoroacetyl)aminophenyl group in the hapten is one of the essential epitopes for 6D9.

4.2.4 pH-Dependent Study of Catalytic Antibody 6D9: The pH dependence of antibody 6D9 in the hydrolysis of substrate **6** was examined between pH 6.4 and 11 (Figure 12).[25a] The 6D9-catalyzed reactions above pH 10 could not be followed, due to the rapid spontaneous degradation of the substrate **6**. The catalytic activity of antibody 6D9 shows a linear

Table 4. Kinetic Parameters of the Hydrolysis by Antibody 6D9[a)]

Substrate	Kinetic parameters		
	k_{cat}/min^{-1}	$K_m/\mu M$	k_{cat}/k_{uncat}[b)]
7	0.030	515	20
8	0.033	56	934
9	0.012	255	155

a) Reaction conditions: 25 °C, 10% DMSO/50 mM TrisHCl, pH 8.0. b) The first-order rate constants of the hydrolyses of substrates **7**, **8**, and **9** without antibody (k_{uncat}) were, 1.5×10^{-1}; 3.5×10^{-5}, and 7.5×10^{-5} min^{-1}, respectively.

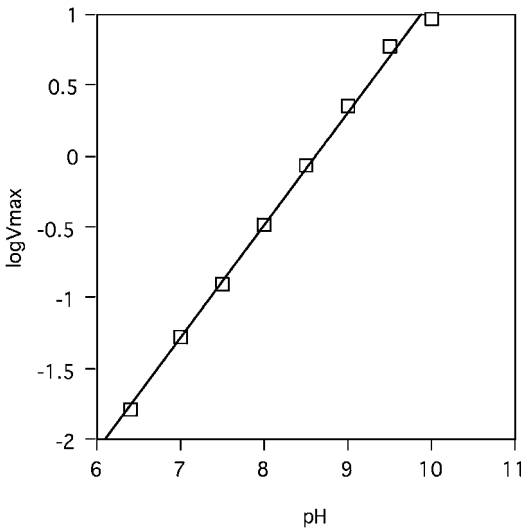

Figure 12. pH dependence of the rate of the catalysis (V_{max}) of substrate **6** hydrolysis by catalytic antibody 6D9.

dependence on hydroxide ion concentration in the pH range. It thus appears that hydroxide ion directly attacks the antibody-bound substrate and the resulting transition state is stabilized in the antibody-combining site.

4.2.5 Thermodynamic Analyses of the Binding of the Catalytic Antibodies: If antibodies catalyze reactions according to the theoretical relationship between the affinity for the transition state and the catalytic efficiency, the ratio of the dissociation constants for the transition-state analog (K_{TSA}) and the corresponding substrate (K_S) should be equal to the rate enhancement ($k_{cat}/k_{uncat} = K_S/K_{TSA}$) as showed in the previous section. An important aspect of transition-state theory is that it relates the rates of a reaction to the difference in Gibbs free energy between the substrate and the transition state. To gain deep understanding of the catalytic mechanism of antibody 6D9, we carried out thermodynamic analyses of the binding of catalytic antibody 6D9 with the transition-state analog (TSA) and the substrate by using isothermal titration calorimetry (ITC).[28] As a reference we chose 9C10. Although the catalytic activity of 9C10 is about ten-fold lower than that of 6D9, both antibodies seem to use the same catalytic mechanism, shown in the transition-state analyses as well as amino acid sequence analyses.

To investigate the binding thermodynamics of antibodies with the substrate by ITC, water-soluble substrate **11** was prepared (Figure 13). The kinetic parameters with substrate **11**

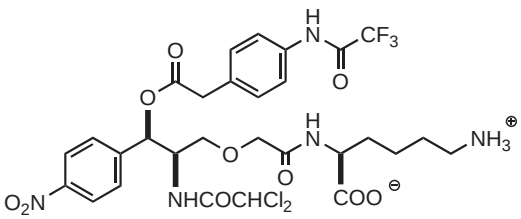

11

Figure 13. The structure of a water-soluble substrate **11** used for the ITC measurement.

Table 5. Thermodynamic Parameters of TSA **5** Binding to 6D9 and 9C10 at 25 °C and pH 6.0

Abs	n	K_a /M^{-1}	ΔG /kJ mol^{-1}	ΔH /kJ mol^{-1}	$T\Delta S$ /kJ mol^{-1}
6D9	1.94	1.32×10^8	−56.32	−38.95	17.36
9C10	1.98	1.07×10^9	−61.46	−78.53	−17.07

Table 6. Thermodynamic Parameters of Substrate **11** Binding to 6D9 and 9C10 at 25 °C and pH 6.0

Abs	n	K_a /M^{-1}	ΔG /kJ mol^{-1}	ΔH /kJ mol^{-1}	$T\Delta S$ /kJ mol^{-1}
6D9	1.97	5.98×10^4	−37.20	−15.73	21.46
9C10	1.99	1.16×10^8	−55.98	−68.78	−12.80

Table 7. Difference in Binding Thermodynamics between the Interaction of the Substrate **11** and Transition-State Analog **5**[a)]

Abs	$\Delta\Delta G$[b)] /kJ mol^{-1}	$\Delta\Delta H$[c)] /kJ mol^{-1}	$T\Delta\Delta S$[d)] /kJ mol^{-1}
6D9	−19.12	−23.22	−4.10
9C10	−5.48	−9.75	−4.27

a) The thermodynamic parameters were determined at 25 °C. b) $\Delta\Delta G = \Delta G_{TSA} - \Delta G_{sub}$. c) $\Delta\Delta H = \Delta H_{TSA} - \Delta H_{sub}$. d) $T\Delta\Delta S = T\Delta S_{TSA} - T\Delta S_{sub}$.

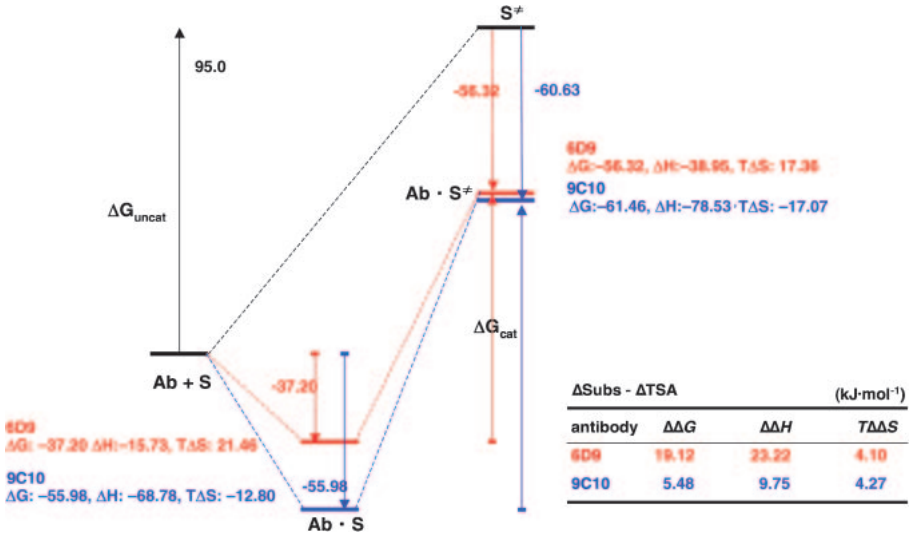

Figure 14. Energy profiles for 6D9- and 9C10-catalyzed reactions and uncatalyzed reaction.

are similar to those of compound **6**, indicating the substrate modification has little effect on the antibody binding. Since the hydrolysis of substrate **11** can be negligible at pH 6 during the ITC measurements, the binding assays were carried out at pH 6.

The results obtained by ITC measurements using TSA **5** and substrate **11** are summarized in Tables 5 and 6, respectively. It should be pointed out that a positive entropy change of 6D9 was observed, which is a unique feature among general antigen–antibody interactions. This result should be due to the large hydrophobic interaction with TSA or the substrate, including the importance of the dehydration effect of water molecules in the binding activity of 6D9.

The differences in the binding thermodynamics between substrate **11** and TSA **5** for 6D9 and 9C10 at 25 °C are summarized in Table 7. The $\Delta\Delta G$ values (the differential binding energy between the TSA and the substrate) of 6D9 and 9C10 are −19.12 and −5.48 kJ mol^{-1}, respectively, both of which are similar to the values calculated based on the k_{cat}/k_{uncat} and the K_S/K_{TSA}. The TSA binding is more stable than the substrate binding, which is in good correlation with the notion that the hydrolysis is accelerated by the differential affinity of the transition state relative to the ground state. We also analyzed $\Delta\Delta G$ by dividing it into $\Delta\Delta H$ and $\Delta\Delta S$, showing that the increased affinity to TSA relative to the substrate is largely due to the favorable $\Delta\Delta H$ (Table 5). Interestingly, although the favorable $\Delta\Delta H$ is partially compensated by $\Delta\Delta S$, the entropic contribution is very limited. Since the ΔH of each hydrogen bond is considered to be lower than 8 kJ mol^{-1},[29] other effects should be involved in the $\Delta\Delta H$ of 6D9 and 9C10, which are −23.22 and −9.75 kJ mol^{-1}, respectively.

Figure 14 shows the energy diagram and the thermodynamic parameters obtained from ITC. As described above, the $\Delta\Delta G$ between binding to the TSA and the substrate **11** in 6D9 is larger than that in 9C10 (Table 7). This difference is mainly due to $\Delta\Delta H$. The larger $\Delta\Delta H$ value of 6D9 relative to that of 9C10 is in good accordance with the larger

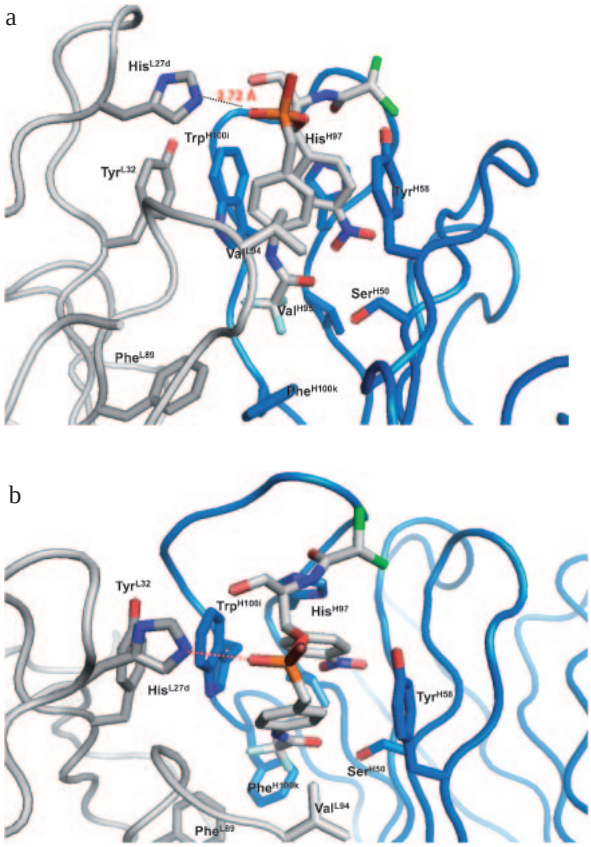

Figure 15. Close-up of the active site of the catalytic antibody 6D9 viewed from the side (a) and from above (b). For clarity, the hapten is represented as the transition-state analog **5**.

k_{cat} value of 6D9. Such correlation between k_{cat} and ΔH suggests "enthalpic strain" in enzyme catalysis, which leads to destabilization of enzyme–substrate complexes.[4,30] If a strain in the substrate is released in the transition state, it contributes to enhancing the value for k_{cat}, but not for k_{cat}/K_m. This change was actually observed in the k_{cat} and K_m for 9C10 and 6D9. This is the first observation that shows the "enthalpic strain" in the catalytic reaction by analyzing equilibrium thermodynamics.

4.3 Structural Analyses of Catalytic Antibody 6D9. In order to understand the mechanistic basis observed in catalytic antibody 6D9, the three-dimensional structure of the catalytic antibody has been solved.[31] Figure 15 show the crystal structure of 6D9 Fab complexed with a transition-state analog. The antibody has a relatively deep cavity and at the bottom of the cavity there is a hydrophobic cavity formed by the hydrophobic residues. A side-chain (N^{ε}) of His^{L27d} is placed in a key position to make a hydrogen bond to the phosphonate oxygen of the transition-state analog with a distance of 2.72 Å. This His^{L27d} is conserved in four catalytic antibodies (6D9, 4B5, 8D11, and 9C10). The site-directed mutagenesis of His^{L27d} to Ala yields no detectable catalytic activity.[32] These results suggest that His^{L27d} in the light chain CDR-1 stabilizes the oxyanionic transition state by a hydrogen bond or electrostatic interaction.

To determine the protonation and deprotonation forms and the tautomeric states of histidine residues (Figure 16) in the Fab fragment of catalytic antibody 6D9 we have also performed NMR experiments using relatively large coupling constants between ^{15}N and ^{13}C in the imidazole ring.[33,34] The identification of the protonation form and the tautomeric states can be achieved by the intensity ratio, I/I_0, of the HSQC cross-peaks with and without the modulation, where I and I_0 are the

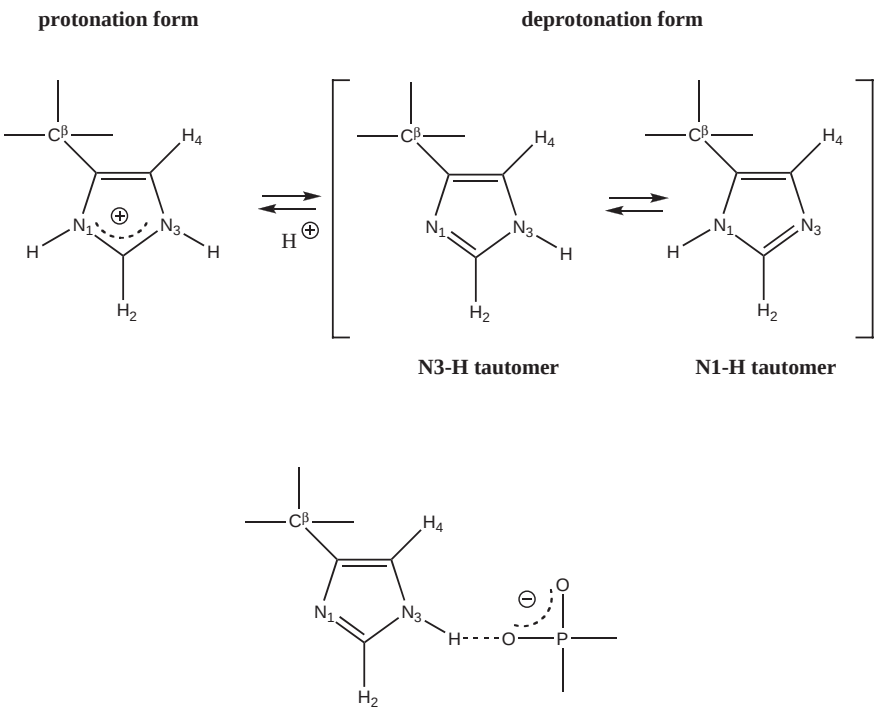

Figure 16. Protonation and deprotonation forms and tautomeric states in imidazole ring of histidine residue.

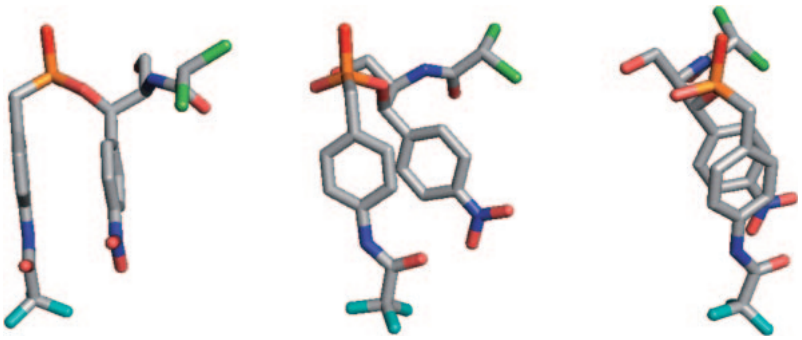

Figure 17. The conformation of the transition-sate analog bound in antibody 6D9, viewed from three different directions.

cross-peak intensities in the ^{1}H–^{13}C CT-HSQC spectra with and without the J_{C-N} amplitude modulation, respectively. Under certain conditions, the values of the intensity ratios, I/I_0, which are calculated from the C2-H and C4-H resonances, are expected to be I/I_0 (C2-H) = 0.45–0.65 and 0.016 for the deprotonation and protonation state, respectively, and I/I_0 (C4-H) = 0.36 and 0.91 for the N3-H and N1-H tautomers, respectively. For His^{L27d}, which is largely responsible for the catalytic activity of 6D9, the obtained value of the intensity ratios, I/I_0, which are calculated from the C2-H and C4-H resonances, are 0.68 and 0.27, respectively. On the basis of these values, it is concluded that the chemical forms of His^{L27d} correspond to the deprotonation form and that the equilibrium between the tautomers for His^{L27d} lies toward the N3-H tautomer significantly. It is suggested that His^{L27d} stabilizes the transition-state analog in the complex through a hydrogen bond between the imidazole ring and the transition state analog. The hydrogen bond might also stabilize the N3-H tautomer of His^{L27d}.

In the antibody–hapten complex, the hapten bears a folded conformation and the two-stacked aromatic rings in the hapten are buried deep in the antigen-combining site through aromatic–aromatic interaction with Trp^{H100i} and Tyr^{H58}. Figure 17 show a conformation of the transitions-state analog bound in antibody 6D9. The conformation of the bound hapten suggests the antibody binds the substrate to change the conformation of the ester moiety to a thermodynamically unstable non-planar conformation, thereby making it easy for the substrate to reach the transition state during catalysis. It is well known that the planar Z form is the most stable conformation in esters.[35] Given that the substrate is bound to the antibody 6D9 in the same manner as the TSA binding, the ester no longer possess the conformation of the most stable Z form. The conformational change of the ester moiety from a stable Z form to an unstable twisted conformation leads to a weak substrate binding affinity of the antibody. The transition-state stabilization observed in 6D9-catalyzed hydrolysis is likely due to the perturbation between the intrinsic binding energy to the transition state and the weak binding to the substrate.

The substrate specificity of the antibody 6D9 can readily be understood from the detailed image of the antigen-combining site obtained from structural analyses. Replacement of the nitro group with a dichloroacetamido substituent resulted in a substrate that was not catalyzed by 6D9. The crystal structure shows that this modification cannot be accommodated, due to steric conflict with the binding pocket. Since the trifluoroacetyl group of the transition-state analog was buried deep in the antigen-combining site, where it functions as an important epitope for the entire binding affinity, the substitution of the trifluoroacetyl group for an acetyl group causes a reduced catalytic activity. Any changes in the appendage at C-3 of the substrate are tolerated, which is consistent with the solvent exposed position seen in the crystal structures.

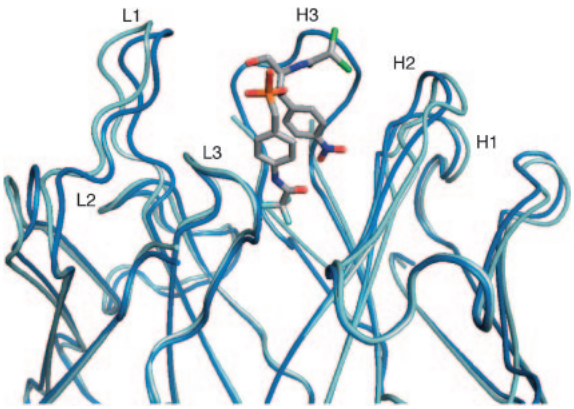

Figure 18. A schematic drawing of the liganded (blue) and unliganded (sky blue) form of the TSA binding site. The Fv domain of the unliganded form is superimposed on that of the liganded form. The six CDR loops (L1–L3 and H1–H3) are labeled. For clarity, the hapten is represented as the transition-state analog **5**.

We have also determined the crystal structure of unliganded 6D9 Fab and compared it to that of TSA-liganded 6D9 Fab (Figure 18). The most prominent differences in the CDR loop structure between the unliganded and liganded structures are in the CDR H3 loop. In the unliganded structure, the electron density corresponding to the loop is very week and not interpretable, suggesting it is severely disordered. In contrast, the same loop in the liganded structure has clear electron density and plays an essential role in TSA recognition in the complex. Thus, the H3 loop has well-defined structure only when the TSA is present. The CDR L1 loop is apparently more mobile in the unliganded form. The L1 loop contains the catalytic residue, His^{L27d}. It is, therefore, very likely that the hydrogen bond between His^{L27d} and the TSA stabilizes the structure of this loop in the complex (Figure 19a).

There are two notable differences in the hydrophobic antigen-combining site of the liganded and unliganded antibodies. The first is Trp^{H100i} at the bottom of the H3 loop (Figure 19b).

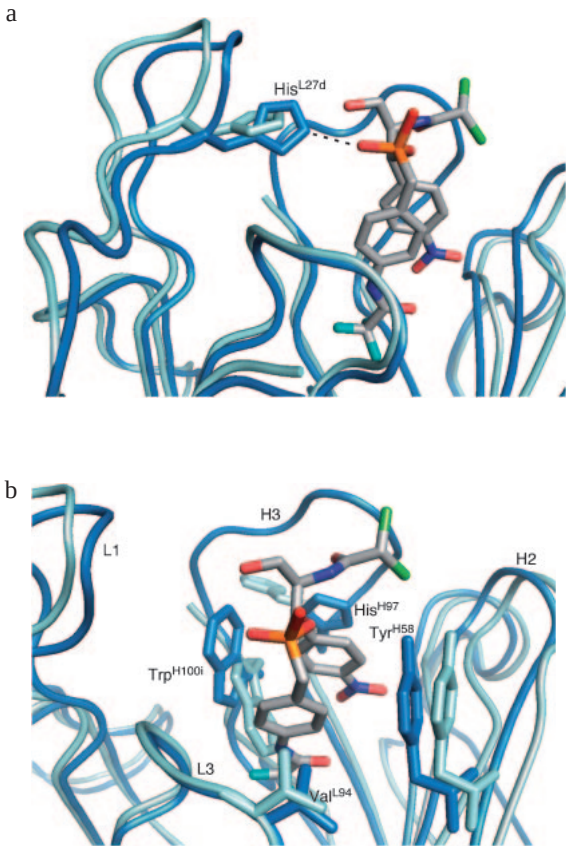

Figure 19. Conformational changes of His^{L27d} (a) and Trp^{H100i} (b) induced by TSA binding. The structures 6D9 in the unliganded form (sky blue) are superimposed on that of the liganded form (blue). Binding of the TSA "pulls" the L1 loop through a hydrogen bond between the phosphonate and the catalytic His^{L27d}. The indole ring of Trp^{H100i} in the unliganded form occupies a hydrophobic pocket, whereas it flips out to allow the TSA to bind in the pocket in the complex. For clarity, the hapten is represented as the transition-state analog **5**.

The indole ring points toward the molecular surface in the complex to accommodate the TSA, but in the unliganded structure, the side-chain rotates around the $\chi 1$ angle to fill the hydrophobic binding pocket. The second difference is residue His^{H97}, also at the bottom of the H3 loop (Figure 19b). The imidazole ring directly stacks on the nitrobenzene moiety of the TSA in the complex, but leaves from the binding pocket in the unliganded structure.

4.4 Reaction Mechanism of Catalytic Antibodies. The kinetic and transition-state analyses showed, as expected from the immunized with TSA **5**, that antibody 6D9 stabilized the transition state, produced by the direct attack of a hydroxy anion to the ester carbonyl in the antibody-catalyzed hydrolysis. Furthermore, the X-ray structural analysis and the site-directed mutagenesis of 6D9 defined a catalytic residue, histidine at 27d in the light chain CDR1 (His^{L27d}), which was placed in a key position to form a hydrogen bond to the transition-state structure. Although the role of histidine as a nucleophilic and general base catalyst in ester hydrolysis is well established, the kinetic studies might rule out the possibility of the histidine functioning as a nucleophilic and general base catalyst in the antibody-catalyzed hydrolysis. Antibody 6D9 turned over several hundred fold with the substrate, without either burst kinetic or noticeable reaction inhibition, and the pH profile of antibody 6D9 shows a linear dependence on hydroxide ion concentration between pH 6.0 and 10.0. In addition, thermodynamic analyses indicate that "enthalpic strain" contributes to increase the differential affinity between the transition state and the ground state. One of the factors contributing to enthalpic strain may be a conformational change in the substrate. In the structure of the 6D9-TSA complex, the transition-state analog has a folded conformation, and the two aromatic rings are buried beep in the antigen-combining site through aromatic–aromatic interactions with Trp^{H100i} and Tyr^{H58}. The conformation of the bound TSA suggests that the antibody binds the substrate to change the conformation of the ester moiety to a thermodynamically unstable twisted conformation. Thus, the conformational change of the ester moiety to the twisted conformation probably results in the experimentally observed weak binding affinity of the substrate for 6D9. The large hydrophobic interaction can induce a global conformational change of the antibody and constraint on the substrate, generating more efficient catalysis. Figure 20 shows the catalytic mechanism of 6D9 in the hydrolysis of an ester substrate.

Comparison of the amino acid sequences between 6D9 and 9C10 also suggests the difference in catalytic activity between them. The H3 loop of 9C10 is five residues shorter than that of 6D9 and is missing Trp^{H100i}, the key residue for the binding of the transition-state analog in 6D9. As described above, in the 6D9-TSA complex, the two aromatic rings of the TSA are stacked in association with Trp^{H100i} and Tyr^{H58}, suggesting that these residues contribute to the conformational strain on the substrate. Thus, 9C10 lacks the important aromatic–aromatic interaction, resulting in decreased strain on the substrate. This explanation for the catalytic activity is supported by the difference in the thermodynamic properties between 6D9 and 9C10. Figure 21 summarizes the catalytic mechanism of 9C10 in the hydrolysis of an ester substrate.

5. Conclusion

In this study, we have examined the molecular mechanism of catalytic antibody 6D9, which was generated against a phosphonate transition-state analog. The antibody 6D9 uses transition-state stabilization as a major catalytic mechanism, which is expected from designing the transition-state analog. Catalytic antibodies are still much inferior to natural enzymes in their catalytic efficiency. This is because catalytic antibodies are elicited against a single specific structure; by contrast, enzymes have evolved to recognize a series of structures that connect the substrate and the product along the reaction coordinate. However, several aspects including the mechanism of enzyme catalysts can be faithfully mimicked. In addition, there is an advantage of using catalytic antibodies in that both substrates and transition-state analogs are available to study catalytic mechanisms. Therefore, the molecular mechanism of catalytic antibodies might provide useful insights to understanding catalysis in enzymes. The present mechanistic studies might provide the basis of the new design of haptens for highly efficient catalytic antibodies.

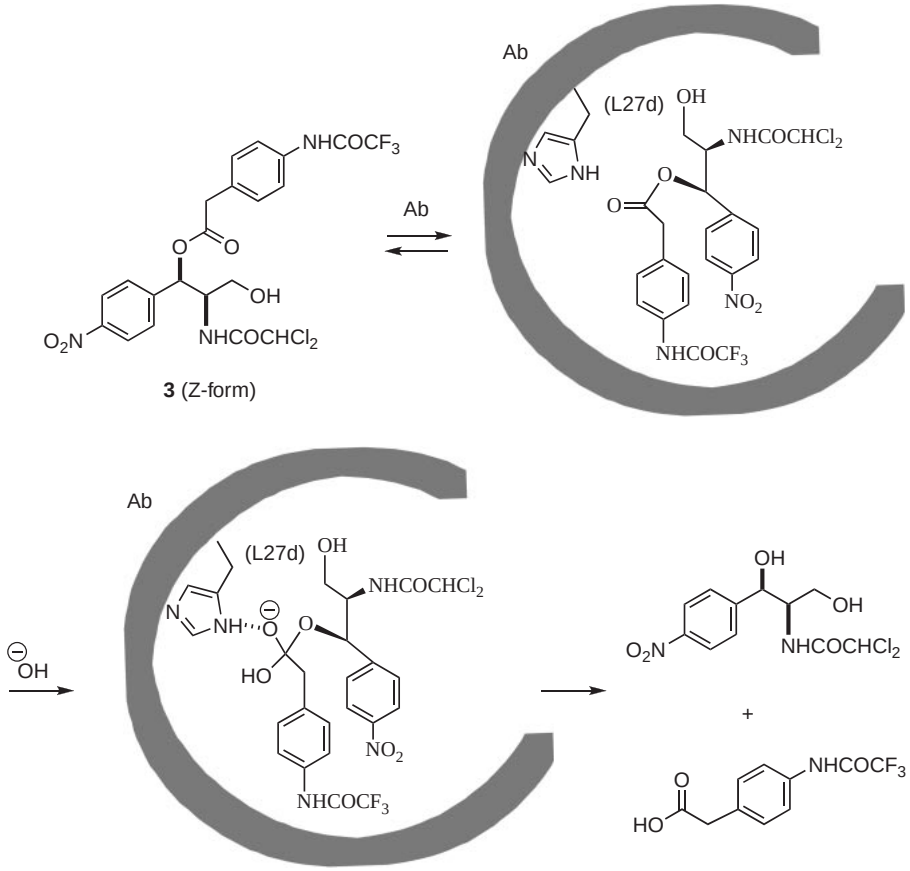

Figure 20. Catalytic mechanism of antibody 6D9 in the hydrolysis of ester **3**.

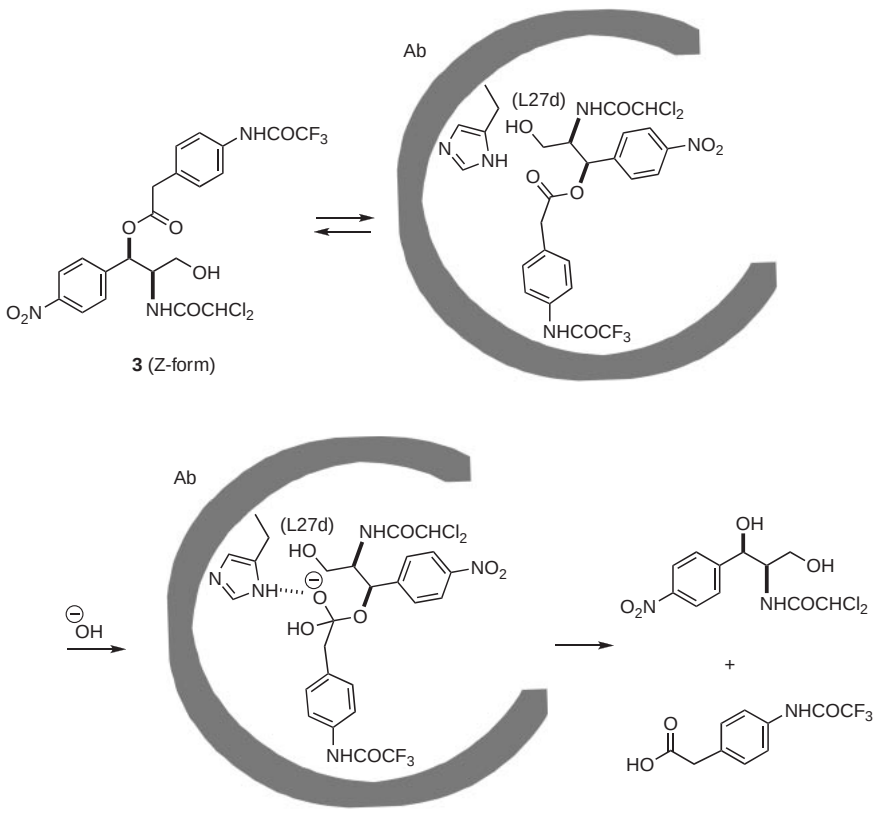

Figure 21. Catalytic mechanism of antibody 9C10 in the hydrolysis of ester **3**.

We wish to thank with great pleasure the many collaborators who are listed in the references. They have contributed experimentally as well as conceptually to the elucidation of the molecular mechanism of transition-state stabilization in catalytic antibodies summarized in the accounts. This research was supported in part by a Grant-in-Aid for Scientific Research from the Ministry of Education, Culture, Sports, Science and Technology of Japan, and the Asahi Glass Foundation.

References

1 L. Pauling, *Chem. Eng. News* **1946**, *24*, 1375.
2 L. Pauling, *Am. Sci.* **1948**, *36*, 51.
3 L. Pauling, *Nature* **1948**, *161*, 707.
4 W. P. Jencks, *Catalysis in Chemistry and Enzymology*, McGraw Hill, New York, **1969**.
5 A. Tramontano, K. D. Janda, R. A. Lerner, *Science* **1986**, *234*, 1566.
6 S. J. Pollack, J. W. Jacobs, P. G. Schultz, *Science* **1986**, *234*, 1570.
7 For reviews: a) R. A. Lerner, S. J. Benkovic, P. G. Schultz, *Science* **1991**, *252*, 659. b) P. G. Schultz, R. A. Lerner, *Science* **1995**, *269*, 1835. c) C. M. Blackburn, A. Datta, H. Denham, P. Wentworth, Jr., *Adv. Phys. Org. Chem.* **1998**, *31*, 250. d) A. J. Kirby, *Acta Chem. Scand.* **1996**, *50*, 203. e) P. Wentworth, K. D. Janda, *Curr. Opin. Chem. Biol.* **1998**, *2*, 138. f) D. Hilvert, *Annu. Rev. Biochem.* **2000**, *69*, 751. g) F. Tanaka, *Chem. Rev.* **2002**, *102*, 4885. h) T. Tsumuraya, I. Fujii, *J. Synth. Org. Chem., Jpn.* **2006**, *64*, 1159.
8 *Catalytic Antibodies*, ed. by E. Kainan, Wiley-VCH, Weinheim, **2005**.
9 F. M. Burnet, *The Clonal Selection Theory on Evolution*, Oxford University Press, Cambridge, **1959**.
10 W. Gilbert, *Nature* **1978**, *271*, 501.
11 D. W. Talmage, *Science* **1959**, *129*, 1643.
12 S. Tonegawa, *Nature* **1983**, *302*, 575.
13 C. A. Janeway, Jr., P. Travers, *Immunobiology, the Immunosystem in Health and Disease*, Current Biology Ltd., London, **1997**.
14 a) A. Fersht, *Enzyme Structure and Mechanism*, W. H. Freeman and Company, New York, **1985**. b) A. Fersht, *Structure and Mechanism in Protein Science*, W. H. Freeman and Company, New York, **2002**.
15 a) H. Eyring, *J. Chem. Phys.* **1935**, *3*, 107. b) H. Eyring, *Chem. Rev.* **1935**, *17*, 65.
16 J. W. Jacobs, *Nat. Biotechnol.* **1991**, *9*, 258.
17 J. D. Stewart, S. J. Benkovic, *Nature* **1995**, *375*, 388.
18 M. M. Mader, P. A. Bartlet, *Chem. Rev.* **1997**, *97*, 1281.
19 K. Teraishi, M. Saito, I. Fujii, H. Nakamura, *Tetrahedron Lett.* **1992**, *33*, 7153.
20 a) A. Tramontano, A. A. Ammann, R. A. Lerner, *J. Am. Chem. Soc.* **1988**, *110*, 2282. b) J. Jacobs, P. G. Schultz, R. Sugasawara, M. Powell, *J. Am. Chem. Soc.* **1987**, *109*, 2174. c) S. J. Pollack, P. Hsiun, P. G. Schultz, *J. Am. Chem. Soc.* **1989**, *111*, 5961.
21 a) K. D. Janda, D. Schloeder, S. J. Benkovic, R. A. Lerner, *Science* **1988**, *241*, 1188. b) S. J. Benkovic, J. A. Adams, C. L. Borders, Jr., K. D. Janda, R. A. Lerner, *Science* **1990**, *250*, 1135. c) R. A. Gibbs, P. A. Benkovic, K. D. Janda, R. A. Lerner, S. J. Benkovic, *J. Am. Chem. Soc.* **1992**, *114*, 3528. d) M. T. Martin, T. S. Angeles, R. Sugasawara, N. I. Aman, A. D. Napper, M. J. Darsley, R. I. Sanchez, P. Booth, R. C. Titmas, *J. Am. Chem. Soc.* **1994**, *116*, 6508. e) C. Gao, B. J. Lavey, C.-H. L. Lo, A. Datta, P. Wentworth, Jr., K. D. Janda, *J. Am. Chem. Soc.* **1998**, *120*, 2211. f) O. Ersoy, R. Fleck, A. Sinskey, S. Masamune, *J. Am. Chem. Soc.* **1998**, *120*, 817.
22 a) K. D. Janda, M. I. Weinhouse, D. M. Schloeder, R. A. Lerner, S. J. Benkovic, *J. Am. Chem. Soc.* **1990**, *112*, 1274. b) K. D. Janda, M. I. Weinhouse, T. Danon, K. A. Pacelli, D. M. Schloeder, *J. Am. Chem. Soc.* **1991**, *113*, 5427. c) M. T. Martin, A. D. Napper, P. G. Schultz, A. R. Ress, *Biochemistry* **1991**, *30*, 9757. d) K. D. Janda, J. A. Ashley, T. M. Jones, D. A. McLeod, D. M. Schloeder, M. I. Weinhouse, R. A. Lerner, R. A. Gibbs, P. A. Benkovic, R. Hilhorst, S. J. Benkovic, *J. Am. Chem. Soc.* **1991**, *113*, 291. e) K. D. Janda, S. J. Benkovic, R. A. Lerner, *Science* **1989**, *244*, 437. f) D. S. Tawfik, B. S. Green, R. Chap, M. Sela, Z. Eshhar, *Proc. Natl. Acad. Sci. U.S.A.* **1993**, *90*, 373. g) Y. Iwabuchi, Y. Miyashita, R. Tanimura, K. Kinoshita, M. Kikuchi, I. Fujii, *J. Am. Chem. Soc.* **1993**, *90*, 5337. h) G. W. Zhou, J. Guo, W. Huang, R. J. Fletterick, T. S. Scanlan, *Science* **1994**, *265*, 1059. i) T. Tsumuraya, H. Suga, S. Meguro, A. Tsunakawa, S. Masamune, *J. Am. Chem. Soc.* **1995**, *117*, 11390. j) S. Kurihara, T. Tsumuraya, K. Suzuki, M. Kuroda, L. Liu, Y. Takaoka, I. Fujii, *Chem.—Eur. J.* **2000**, *6*, 1656. k) T. Tsumuraya, N. Takazawa, A. Tsunakawa, R. Fleck, S. Masamune, *Chem.—Eur. J.* **2001**, *7*, 3748.
23 H. Miyashita, Y. Karaki, M. Kikuchi, I. Fujii, *Proc. Natl. Acad. Sci. U.S.A.* **1993**, *90*, 5337.
24 P. Wentworth, A. Datta, D. Blakey, T. Boyle, L. J. Partridge, G. M. Blackburn, *Proc. Natl. Acad. Sci. U.S.A.* **1996**, *93*, 799.
25 a) I. Fujii, F. Tanaka, H. Miyashita, R. Tanimura, K. Kinoshita, *J. Am. Chem. Soc.* **1995**, *117*, 6199. b) N. Takahashi, H. Kakinuma, L. Liu, Y. Nishi, I. Fujii, *Nat. Biotechnol.* **2001**, *19*, 563. c) B. Gigant, T. Tsumuraya, I. Fujii, M. Knossow, *Structure* **1999**, *7*, 1385.
26 a) P. A. Bartlett, C. K. Marlowe, *Biochemistry* **1983**, *22*, 4618. b) R. C. Thompson, C. A. Bauer, *Biochemistry* **1979**, *18*, 1552. c) K. Brady, R. H. Abeles, *Biochemistry* **1990**, *29*, 7608. d) J. O. Westerik, R. Wolfenden, *J. Biol. Chem.* **1972**, *247*, 8195. e) R. C. Thompson, *Biochemistry* **1973**, *12*, 47. f) J. E. Hanson, A. P. Kaplan, P. A. Bartlett, *Biochemistry* **1989**, *28*, 6294. g) H. K. Nair, J. Seravalli, T. Arbuckle, D. M. Quinn, *Biochemistry* **1994**, *33*, 8566.
27 H. Miyashita, T. Hara, R. Tanimura, F. Tanaka, M. Kikuchi, I. Fujii, *Proc. Natl. Acad. Sci. U.S.A.* **1994**, *91*, 6045.
28 M. Oda, N. Ito, T. Tsumuraya, K. Suzuki, M. Sakakura, I. Fujii, *J. Mol. Biol.* **2007**, *369*, 198.
29 *Biological Microcalorimetry*, ed. by M. Eftnik, R. Biltonen, A. E. Beezer, Acadamic Press, New York, **1980**, p. 343.
30 T. C. Bruice, S. J. Benkovic, *Biochemistry* **2000**, *39*, 6267.
31 O. Kristensen, D. G. Vassylyev, F. Tanaka, K. Morikawa, I. Fujii, *J. Mol. Biol.* **1998**, *281*, 501.
32 H. Miyashita, T. Hara, R. Tanimura, S. Fukuyama, C. Cagnon, A. Kohara, I. Fujii, *J. Mol. Biol.* **1997**, *267*, 1247.
33 N. Shimba, H. Takahashi, M. Sakakura, I. Fujii, I. Shimada, *J. Am. Chem. Soc.* **1998**, *120*, 10988.
34 M. Sakakura, H. Takahashi, N. Shimba, I. Fujii, I. Shimada, *J. Mol. Biol.* **2007**, *367*, 133.
35 P. Deslongchamps, *Stereoelectronic Effects in Organic Chemistry*, Pergamon Press, Oxford, **1983**.

Takeshi Tsumuraya is an Associate Professor of Osaka Prefecture University. He studied group 14 organometallic chemistry at University of Tsukuba where he completed his doctoral work in 1990 under the direction of Professor Wataru Ando. After working as a postdoctoral research associate at the Massachusetts Institute of Technology with Professor Satoru Masamune, he worked as a senior research scientist at the Kao Institute for Fundamental Research, where he studied catalytic antibodies. He joined, in 1997, the Biomolecular Engineering Research Institute in Suita, Osaka as a principal research scientist, and stayed there until he moved in 2003 to his present location, Osaka Prefecture University. His interests are in the areas of catalytic antibodies, antibody and enzyme engineering, and peptide science.

Ikuo Fujii is a Professor of Biological Science, Osaka Prefecture University. He earned his Ph.D. in pharmaceutical science under the direction of Professor Ken Kanematsu at Kyushu University in 1986, and then he was an assistant professor at Kyushu University. He was a postdoctoral associate in the laboratory of Professor Emil T. Kaiser at Rockefeller University from 1988–1989. He moved to the Scripps Research Institute to work with Professor Richard A. Lerner in 1989. In 1991, he was appointed as a senior research scientist to direct the antibody engineering group in Protein Engineering Research Institute (PERI). He moved to Biomolecuar Engineering Research Institute (BERI) and was promoted to Research Director in the Department of Bioorganic Chemistry in 1996. In 2003, he was appointed as Professor at Osaka Prefecture University. In 1996, he received The Pharmaceutical Society of Japan Award for Young Scientists for his contribution in the field of catalytic antibodies.